BIOCHEMISTRY
including biophysical chemistry & molecular biology

Article

pubs.acs.org/biochemistry

Investigation of the Curvature Induction and Membrane Localization of the Influenza Virus M2 Protein Using Static and Off-Magic-Angle Spinning Solid-State Nuclear Magnetic Resonance of Oriented Bicelles

Tuo Wang and Mei Hong*

Department of Chemistry, Massachusetts Institute of Technology, 170 Albany Street, Cambridge, Massachusetts 02139, United States

Supporting Information

ABSTRACT: A wide variety of membrane proteins induce membrane curvature for function; thus, it is important to develop new methods to simultaneously determine membrane curvature and protein binding sites in membranes with multiple curvatures. We introduce solid-state nuclear magnetic resonance (NMR) methods based on magnetically oriented bicelles and off-magic-angle spinning (OMAS) to measure membrane curvature and the binding site of proteins in mixed-curvature membranes. We demonstrate these methods on the influenza virus M2 protein, which not only acts as a proton channel but also mediates virus assembly and membrane scission. An M2 peptide encompassing the transmembrane (TM) domain and an amphipathic helix, M2(21−61), was studied and compared with the TM peptide (M2TM). Static ^{31}P NMR spectra of magnetically oriented 1,2-dimyristoyl-*sn*-glycero-3-phosphocholine (DMPC)/1,2-dihexanoyl-*sn*-glycero-3-phosphocholine (DHPC) bicelles exhibit a temperature-independent isotropic chemical shift in the presence of M2(21−61) but not M2TM, indicating that the amphipathic helix confers the ability to generate a high-curvature phase. Two-dimensional (2D) ^{31}P spectra indicate that this high-curvature phase is associated with the DHPC bicelle edges, suggestive of the structure of budding viruses from the host cell. ^{31}P- and ^{13}C-detected ^{1}H relaxation times of the lipids indicate that the majority of M2(21−61) is bound to the high-curvature phase. Using OMAS experiments, we resolved the ^{31}P signals of lipids with identical headgroups based on their distinct chemical shift anisotropies. On the basis of this resolution, 2D ^{1}H−^{31}P correlation spectra show that the amide protons in M2(21−61) correlate with the DMPC but not DHPC ^{31}P signal of the bicelle, indicating that a small percentage of M2(21−61) partitions into the planar region of the bicelles. These results show that the amphipathic helix induces high membrane curvature and localizes the protein to this phase, in good agreement with the membrane scission function of the protein. These bicelle-based relaxation and OMAS solid-state NMR techniques are generally applicable to curvature-inducing membrane proteins such as those involved in membrane trafficking, membrane fusion, and cell division.

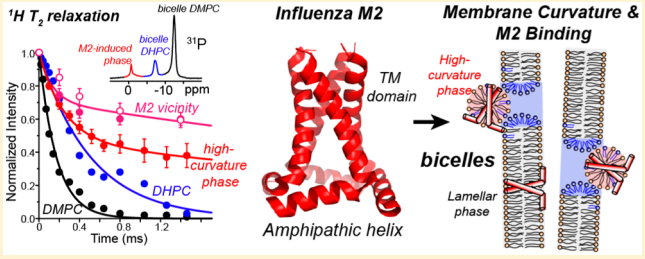

Many membrane proteins cause membrane curvature to conduct functions such as membrane trafficking,[1] endocytosis,[2] virus−cell fusion,[3−5] and virus budding.[6,7] Membrane curvature has so far been mainly characterized using electron microscopy[6,8] and small-angle X-ray scattering (SAXS).[9] However, these techniques do not have the ability to determine the high-resolution structure of the proteins involved in curvature induction. Solid-state nuclear magnetic resonance (SSNMR) spectroscopy can in principle simultaneously reveal membrane curvature, protein conformation, and protein−lipid interactions.[5,10−12] The protein and lipid NMR signals can be readily distinguished by detecting ^{13}C and ^{15}N signals for the former and ^{31}P and ^{2}H signals for the latter, and correlation of the two provides information about protein−lipid interactions.[10,11,13] It is therefore of interest to develop new SSNMR techniques to determine membrane curvature, protein structure, and protein−lipid interactions.

To investigate curvature-dependent protein−lipid interactions, it is desirable to use a lipid membrane with defined curvatures and a complexity lower than that of the cell membrane and virus envelope, because the full complement of lipids that commonly exists in eukaryotic membranes may obscure the interactions of the protein with a small subset of lipids to cause curvature. Bicelles present an appealing membrane-mimetic system for elucidating the curvature-inducing propensity of membrane proteins. As bilayered discoidal aggregates formed by mixtures of long-chain and short-chain lipids, bicelles have been widely used in solution and solid-state NMR studies of protein structure.[14−19] By varying the ratios of long-chain to short-chain lipids, one can produce either weakly aligned isotropic bicelles or strongly

Received: February 7, 2015
Revised: March 12, 2015
Published: March 16, 2015

DOI: 10.1021/acs.biochem.5b00127
Biochemistry 2015, 54, 2214−2226

aligned anisotropic bicelles to obtain orientational constraints of proteins that are either distributed between bicelles or embedded within bicelles. For SSNMR studies, anisotropic bicelles are usually used. These bicelles are aligned with the planes parallel to the external magnetic field[15] because of their negative anisotropy of magnetic susceptibility. When paramagnetic lanthanide ions[20] or lipids with phenyl rings[21] are added, the bicelle planes can be flipped to be perpendicular to the magnetic field. Compared to mechanically aligned membranes, the magnetically aligned bicelles are easy to prepare, hydrate, and stabilize for SSNMR structural studies. The morphology of magnetically oriented bicelles has been extensively studied and variously described as disc-shaped,[22] perforated lamellar bilayers,[23] or wormlike micelles.[24] All these models agree about the coexistence of low- and high-curvature domains in the bicelles, with the planar surface dominated by long-chain lipids while the round edges are composed of short-chain lipids. Moreover, the short-chain lipids can exchange between these two domains.[25]

The M2 protein of influenza A viruses is a multifunctional protein that acts at several stages of the virus life cycle. M2 has so far been predominantly studied as a drug-targeted proton channel,[26−30] which manifests its activity after the virus is endocytosed into the host cell, where the low pH of the endosome opens the channel to acidify the virion and cause virus uncoating.[31] Amantadine and rimantadine inhibit the channel by binding to the transmembrane (TM) pore.[27,32] In a later stage of the virus life cycle, when a newly assembled virus is ready to be released from the host cell, M2 is recruited to the neck of the budding virus and mediates membrane scission. Electron microscopy data indicate that this second function is conducted by an amphipathic helix (AH) in the cytoplasmic domain of the protein which causes high membrane curvature:[6] a peptide corresponding to the AH domain is sufficient to bud into giant unilamellar vesicles, and mutations of the AH domain in full-length M2 inhibit vesicle budding in vitro and prevent virus release in vivo. SAXS data further showed that AH-containing M2 peptides incur bicontinuous cubic phases in phosphoethanolamine-rich lipid membranes,[7] consistent with the curvature-inducing function.

In this work, we explore oriented bicelles as a medium to develop new SSNMR methods for investigating the preferential localization of proteins in membrane domains with distinct curvatures. Using the influenza M2 protein, we show that it is possible to measure the protein binding site in low- and high-curvature membranes by detecting lipid dynamics in the vicinity of the protein and by two-dimensional (2D) ^{31}P−^{1}H correlation experiments. Because magic-angle spinning (MAS) NMR spectra cannot resolve the ^{31}P isotropic chemical shifts of lipids with the same headgroup, we introduce off-magic-angle spinning (OMAS) experiments to resolve ^{31}P signals based on the motionally averaged ^{31}P chemical shift anisotropies (CSAs) of long-chain and short-chain lipids. We find that an AH-containing M2 peptide both induces and partitions into a high-curvature membrane phase, thus providing nanometer-scale structural evidence of the membrane scission function of this protein.

EXPERIMENTAL PROCEDURES

Membrane Sample Preparation. Two M2 peptides, M2(22−46) and M2(21−61), were synthesized using Fmoc chemistry and purified by PrimmBiotech (Cambridge, MA). M2(21−61) contains both the TM domain (residues 22−46) and the AH domain (residues 47−61). Uniformly ^{13}C- and ^{15}N-labeled residues were incorporated at L26, V27, A30, G34, and I35 in M2(21−61). For simplicity, we interchangeably denote M2(22−46) as M2TM and M2(21−61) as M2TM-AH in this paper.

1,2-Dimyristoyl-*sn*-glycero-3-phosphocholine (DMPC) and 1,2-dihexanoyl-*sn*-glycero-3-phosphocholine (DHPC) were used to prepare most of the oriented bicelle samples in this study. Following the literature,[33] we dissolved DHPC in ∼45 μL of pH 7.5 Tris buffer and pipetted the solution to a dry powder of the peptide. The mixture was vortexed and added to the desired amount of DMPC powder. This ternary mixture was cooled and heated between 0 and 42 °C five to seven times until the sample became homogeneous. The final solution was viscous at room temperature but fluid at 4 °C. For peptide-free control samples, the DHPC solution was directly added to the DMPC powder and subjected to the same cooling−heating cycles. The bicelle samples were transferred to 4 mm MAS rotors for SSNMR experiments. All samples were hydrated to ∼65 wt %, and the DMPC:DHPC:peptide molar ratio was 48:16:1. d_{22}-DHPC was incorporated into some of the bicelles to investigate the effect of the peptides on lipid-chain order. The M2-containing bicelles were stable for about a month, while the peptide-free bicelles were stable for many months. A second bicelle system consisting of DMPC and 1,2-dihexyl-*sn*-glycero-3-phosphocholine (6-O-PC) was also prepared to assess the generality of curvature induction by M2TM-AH.

Solid-State NMR Spectroscopy. SSNMR experiments were conducted on Bruker wide-bore 400 and 600 MHz spectrometers using 4 mm MAS probes. The oriented bicelles were measured under either the static or the spinning condition, and the angle of the rotation axis was varied by ∼7° around the magic angle. Typical radiofrequency (rf) field strengths were 40−50 kHz for ^{31}P and ^{13}C pulses and ∼30 kHz for ^{1}H decoupling. This weak ^{1}H decoupling field was chosen to avoid overheating and dehydrating the bicelles, which would destroy the orientational alignment. For the same reason, most experiments used long recycle delays of 4.5−6.0 s and a slow spinning frequency of 3.5 kHz. All ^{31}P chemical shifts were referenced to the ^{31}P peak of hydroxyapatite at 2.73 ppm, while all ^{13}C chemical shifts were externally referenced to the adamantane CH_2 signal at 38.48 ppm on the TMS scale.

Static ^{31}P direct polarization (DP) spectra were measured as a function of temperature from 283 to 312 K. To obtain stable alignment, we kept the bicelles in the magnetic field at 312 K for 1 h and further stabilized them for 30 min at each temperature before measurements. All reported temperatures were thermocouple values calibrated using the ^{207}Pb signal of lead nitrate. Static 2D ^{31}P−^{31}P exchange spectra were measured using long mixing times of 0.5−1.0 s. Bicelle samples with and without M2TM-AH were measured at 297 and 306 K, respectively. These temperatures were chosen so that the two samples have the same DHPC ^{31}P chemical shift.

^{31}P- and ^{13}C-detected ^{1}H T_2 relaxation times were measured using a Hahn echo sequence on the ^{1}H channel, followed by ^{1}H spin diffusion and cross-polarization (CP) to the heteronucleus.[34] Increasing the spin diffusion mixing time (t_m) allows us to detect protons farther from the detected ^{31}P site. To exclude peptide ^{1}H contributions to the ^{13}C-detected ^{1}H T_2 data, we also conducted an experiment in which a ^{13}C−^{1}H dipolar filter of 100 μs was added before the ^{1}H Hahn echo period. This dipolar dephasing period suppresses the ^{1}H magnetization of the rigid peptide while retaining that of the

DOI: 10.1021/acs.biochem.5b00127
Biochemistry 2015, 54, 2214−2226

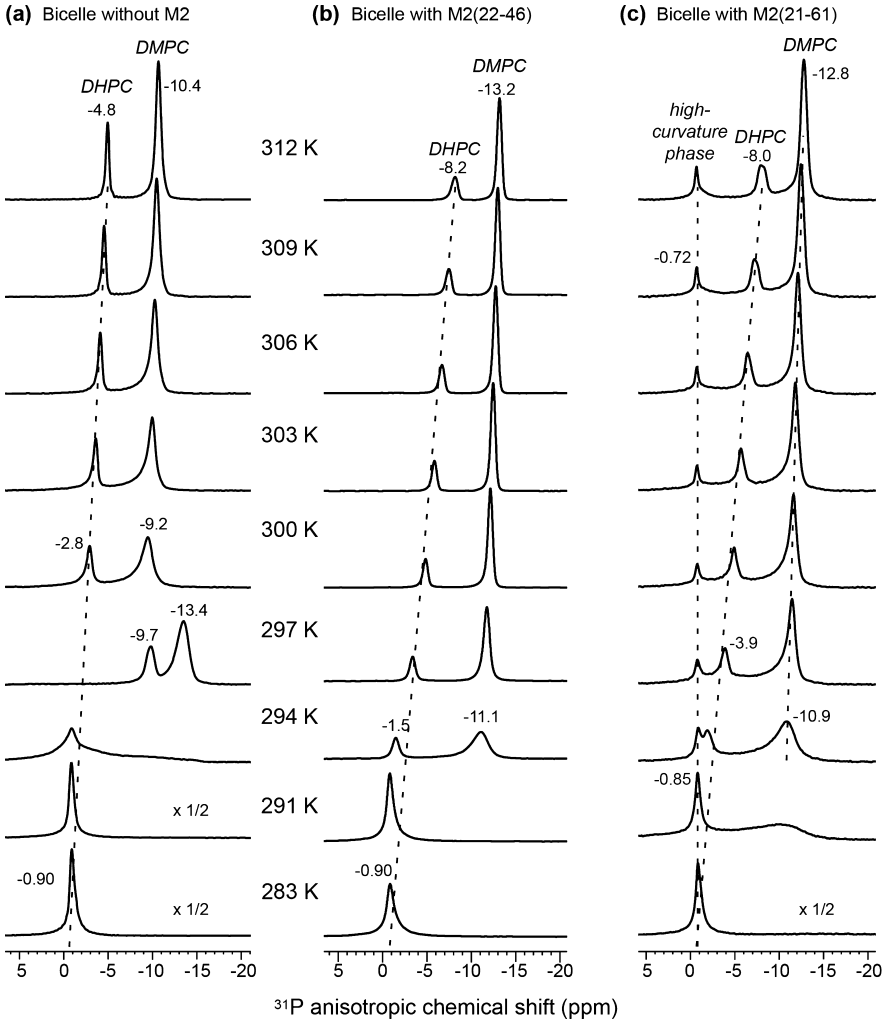

Figure 1. Variable-temperature ^{31}P spectra of static DMPC/DHPC (3:1) bicelles with and without M2. (a) Bicelles without protein. (b) Bicelle with M2TM. (c) Bicelle with M2TM-AH. M2TM-AH creates a temperature-independent isotropic ^{31}P peak, indicating the formation of a high-curvature membrane phase. The other ^{31}P chemical shifts are anisotropic and change with temperature.

mobile lipids and water. The lipid and water ^{1}H T_2 relaxation times were also measured by direct ^{1}H detection at 302 K. ^{2}H quadrupolar echo experiments were conducted on d_{22}-DHPC-containing bicelles to investigate DHPC dynamics in different membranes. A ^{2}H rf field strength of 50 kHz and a recycle delay of 0.8 s were used for these quadrupolar echo experiments.

OMAS experiments were conducted to resolve the ^{31}P chemical shifts of different membrane domains and to obtain high-sensitivity and high-resolution 2D ^{1}H−^{31}P correlation spectra. A spinning frequency of 3.5 kHz was used. This frequency was small enough to avoid perturbing the bicelle morphology but high enough to avoid ^{31}P spinning sidebands.[35] The 2D ^{1}H−^{31}P correlation spectra[13] were measured with MREV-8 ^{1}H homonuclear decoupling during the t_1 evolution period. The ^{1}H 105° pulse length in the MREV-8 pulse train[36] was 6 μs. The ^{1}H chemical shift was calibrated using *N*-formyl-Met-Leu-Phe-OH (MLF), whose ^{1}H chemical shifts have been reported.[37]

RESULTS

Temperature-Dependent Spectra of Peptide-Free DMPC/DHPC Bicelles. ^{31}P NMR is a useful probe of membrane morphology and has been extensively used for studying bicelles. The magnetic alignment of bicelles leads to well-resolved ^{31}P anisotropic chemical shifts under the static condition. From 300 to 312 K, the peptide-free DMPC/DHPC bicelles exhibit two ^{31}P chemical shifts (Figure 1a). The upfield signal at approximately −10 ppm can be assigned to DMPC while the downfield peak can be assigned to DHPC. With increase in temperature, both ^{31}P signals move upfield, but the DHPC chemical shift change (from −2.8 to −4.8 ppm) is larger, making it approach the DMPC signal at high temperature. The DMPC and DHPC chemical shift difference is 6.4 ppm at 300 K and decreases to 5.6 ppm at 312 K. The larger upfield movement of the DHPC ^{31}P peak results from increased exchange of DHPC between the planar and curved regions of bicelles at higher temperatures.[25,38]

At 283−291 K, below the phase transition temperature of DMPC, the ^{31}P spectra exhibit a single peak at the isotropic chemical shift of −0.9 ppm, indicating the formation of a micellar phase or isotropic bicelles.[25,39] At the intermediate temperature of 294 K, a residual power pattern is observed in addition to the isotropic peak, indicating the coexistence of lamellar and isotropic phases. At 297 K, the ^{31}P chemical shifts are discontinuous from the high-temperature values: both DMPC and DHPC peaks moved significantly upfield, to −13.4 and −9.7 ppm, respectively. The DMPC chemical shift is

DOI: 10.1021/acs.biochem.5b00127
Biochemistry 2015, 54, 2214−2226

similar to that of glass-plate-aligned membranes, suggesting that at this temperature the bicelles either are aligned closer to 90° from the magnetic field or have less internal motion and hence higher order parameters. At this temperature, the DHPC ^{31}P peak is only 3.7 ppm downfield from the DMPC peak, indicating that DHPC undergoes significant exchange between the edge and planar regions of the bicelles.

The M2 Amphipathic Helix Generates High Membrane Curvature. The addition of M2TM did not change the qualitative trend of the ^{31}P NMR spectra. Two ^{31}P peaks are observed that move upfield with increasing temperature (Figure 1b). Thus, M2TM does not perturb the bicelle morphology. Above 300 K, the ^{31}P chemical shifts are ~3 ppm more upfield for M2TM-containing bicelles than for peptide-free bicelles. This may be caused by reduced motional amplitudes and thus larger ^{31}P CSAs of the lipids in the presence of M2TM. Between 294 and 297 K, the chemical shift discontinuity and the lamellar phase disappeared, supporting the notion that M2TM stabilizes the bicelles. Both peptide-free and peptide-bound ^{31}P spectra in panels a and b of Figure 1 exhibit DMPC:DHPC ^{31}P area ratios of (3.0 ± 0.3) : 1, which is the same, within experimental uncertainty, as the molar ratio of the lipids in the bicelles, but the M2TM-containing samples show lower height and broader line widths for the DHPC peak, suggesting that M2TM may have slowed DHPC motion.

Interestingly, binding of the AH-containing M2(21−61) peptide caused qualitatively different ^{31}P spectra. In addition to the two anisotropic ^{31}P chemical shifts, a temperature-independent ^{31}P peak at the isotropic frequency of −0.8 ppm is observed from 294 to 312 K (Figure 1c). In general, for nonspinning membrane samples, the ^{31}P CSA is determined by both the chemical structure of the headgroup and lipid reorientational motions. Immobilized lipid headgroups at low temperature give a rigid-limit ^{31}P chemical shift span of ~190 ppm.[40] Fast uniaxial rotational diffusion and wobble of the molecular axis in liquid-crystalline lamellar bilayers average this CSA to ~45 ppm, and the maximal intensity occurs at the upfield edge of the power pattern. This uniaxial ^{31}P chemical shift line shape is further averaged when lipid lateral diffusion and whole-body tumbling are sufficiently fast on the NMR time scale, which occur when the radius of curvature of the membrane is small. Micelles, small vesicles, and bicontinuous cubic phases typically have radii of curvature of 5−30 nm and possess sufficiently high symmetry such that lateral diffusion and tumbling average the ^{31}P CSA to the isotropic value. Thus, the isotropic ^{31}P peak in Figure 1c indicates that M2(21−61) induces a high-curvature membrane phase, which can be micelles, small vesicles, or bicontinuous cubic phases. The temperature independence of this peak frequency is consistent with the symmetry of these phases.

The ^{31}P isotropic peak represents 10−20% of the total ^{31}P intensities (Figure 1c). The lipid composition of the high-curvature phase can be estimated from the ^{31}P peak intensities and the 3:1 DMPC:DHPC total molar ratio. The bicelle DMPC and DHPC peaks in Figure 1c have intensity ratios of (3.0 ± 0.1) : 1; thus, the high-curvature phase has a similar lipid composition to the average composition of this sample. Other bicelle samples prepared in this study had ^{31}P intensity ratios of 2.2:1 to 3.5:1 (data not shown), suggesting that the composition of the high-curvature phase can vary from predominantly DMPC to ~50% DMPC. Because M2TM does not generate this peak, the amphipathic helix is responsible for causing this high-curvature phase. This isotropic peak was also observed in DMPC/6-O-PC bicelles with bound M2TM-AH (Figure S1 of the Supporting Information), indicating that curvature induction is an inherent property of the AH-containing M2 and is independent of the exact composition of the bicelle.

To confirm that the M2(21−61)-induced isotropic ^{31}P peak indeed results from the high curvature of the membrane rather than an accidental magic-angle orientation of the lipid headgroups, we measured the ^{2}H spectra of d_{22}-DHPC, which report lipid-chain dynamics. Bicelles both without and with M2TM-AH were measured. Figure 2 shows that the peptide-free bicelles do not exhibit any zero-frequency peak while the M2TM-AH bound bicelles do; thus, the isotropic ^{31}P peak reflects the curvature of the entire membrane. Consistent with the ^{31}P spectra, the ^{2}H quadrupolar splittings are slightly larger in the M2-containing bicelles than in the peptide-free bicelles, indicating that either the lipid order parameters have increased or the bicelles align closer to 90° from the magnetic field.

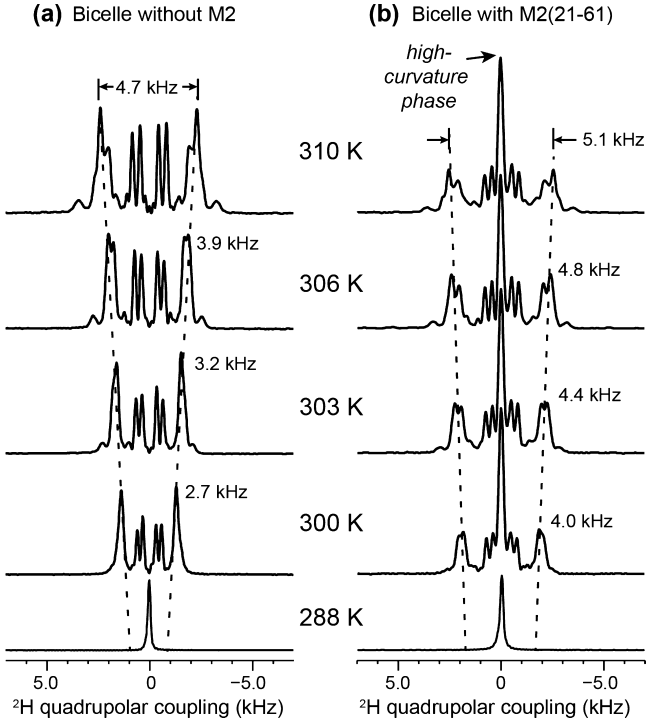

Figure 2. Static ^{2}H spectra of d_{22}-DHPC in DMPC/DHPC bicelles. (a) Bicelles without the peptide. (b) Bicelles with M2TM-AH. The peptide-bound membrane shows a zero-frequency peak, indicating the presence of an isotropic membrane domain or a bicontinuous cubic phase.

To investigate whether the high-curvature membrane phase is in spatial contact with the bicelles, we measured 2D ^{31}P−^{31}P exchange spectra of the M2(21−61)-containing bicelle. At mixing times of 0.5−1.0 s, the spectra exhibit a cross-peak between the isotropic ^{31}P peak and the DHPC peak (Figure 3a,b), indicating that the high-curvature phase is in physical contact with the round edges of the bicelle. At 1.0 s, the cross peak accounts for 20−30% of the diagonal intensity of the high-curvature phase. No cross-peak is observed between DHPC and DMPC. Lipid lateral diffusion over the nanometer dimension of the bicelles occurs on the microsecond time scale, which is sufficiently fast to average out the ^{31}P CSA[41] but

DOI: 10.1021/acs.biochem.5b00127
Biochemistry 2015, 54, 2214−2226

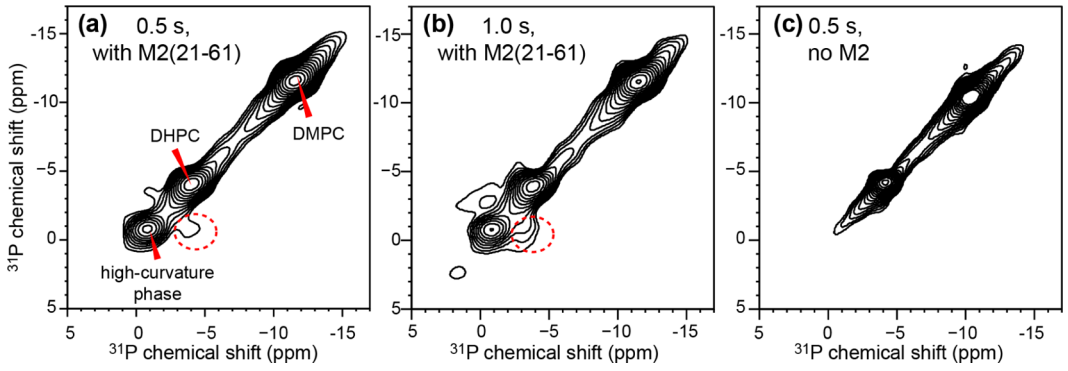

Figure 3. 2D $^{31}P-^{31}P$ exchange spectra of static DMPC/DHPC bicelles. (a) With M2TM-AH and 0.5 s spin diffusion. (b) With M2TM-AH and 1.0 s spin diffusion. (c) Without M2 and with 0.5 s spin diffusion. The spectra were measured at 297 K (a and b) and 306 K (c) to obtain the same DHPC ^{31}P chemical shift. Cross-peaks between the isotropic peak and the DHPC peak (dotted circle) are observed for the protein-bound bicelles in panels a and b.

too short for the millisecond time scale of 2D exchange NMR experiments; thus, the lack of an DMPC/DHPC cross-peak in the 2D spectra is understandable. In a recent study of lipid lateral diffusion using ^{31}P exchange NMR,[42] 200 mM sucrose was added to the membrane to slow the diffusion rate and to permit the detection of lipid reorientations on the millisecond time scale. Similar strategies may be applicable for studying exchange between the edge and planar regions of bicelles, if small-molecule additives that do not affect bicelle alignment can be found.

^{13}C Spectra of M2-Containing DMPC/DHPC Bicelles. Any indirect detection methods for determining the site of protein binding in the mixed-curvature oriented bicelles require the ability to resolve the peptide ^{13}C signals under the static condition. While ^{13}C MAS spectra readily provide this site resolution in terms of isotropic chemical shifts, the resolution of static ^{13}C spectra of membrane peptides with uniformly ^{13}C-labeled residues can be much lower because of $^{13}C-^{13}C$ dipolar coupling. We thus measured the static and MAS ^{13}C spectra of DMPC/DHPC bicelles with and without M2TM-AH to identify and assign the peptide signals. Comparison of the static and MAS spectra allows us to distinguish anisotropic and isotropic chemical shifts, while comparison of peptide-bound and peptide-free bicelles allows us to identify the peptide ^{13}C signals. Temperature variation provides additional clues for resonance assignment by changing the membrane phase and alignment.

Many lipid signals such as glycerol G2 and G1/G3 are detected in the ^{13}C spectra (Figure 4). Their chemical shifts change between 283 K, where the bicelles are in an isotropic phase, and ≥300 K, where the bicelles are oriented. Thus, the high-temperature chemical shifts are anisotropic and the low-temperature shifts are isotropic. This is confirmed by the fact that the 283 K static spectrum matches the MAS spectrum (albeit with broader line widths) while the static high-temperature spectra differ from the MAS spectrum. Two peaks are observed for some of the lipid functional groups in the static spectra, which result from the presence of two different headgroup conformations in phosphocholine and the known conformational differences between the *sn*-1 and *sn*-2 carboxyl carbons.[43] In addition to these lipid signals, the static ^{13}C spectra also exhibit peptide signals such as I35/V27 Cα (65.3 ppm), L26 Cβ (42.2 ppm), V27 Cγ (18.9 ppm), and I35 Cδ1 (10.9 ppm). These anisotropic chemical shifts do not deviate significantly from the isotropic chemical shifts,

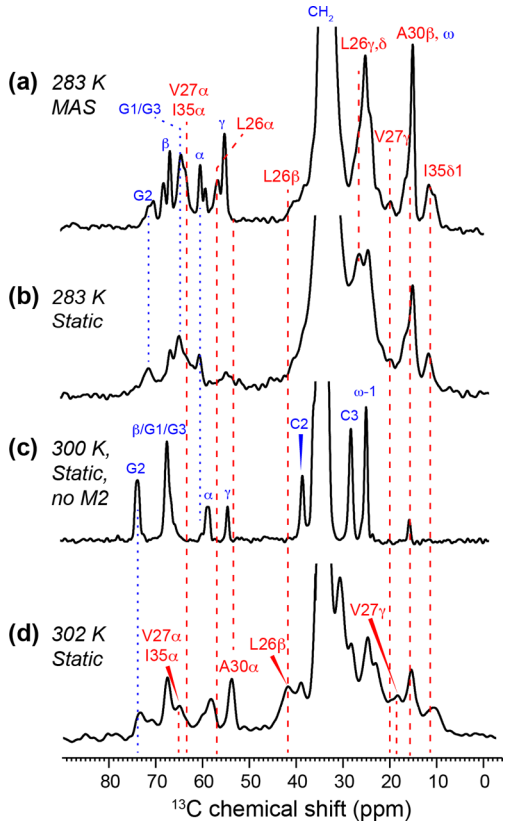

Figure 4. ^{13}C CP spectra of DMPC/DHPC bicelles with and without M2TM-AH under static and MAS conditions. (a) ^{13}C CP spectrum of peptide-bound bicelles at 283 K under MAS, showing resolved protein (red) and lipid (blue) signals at isotropic ^{13}C chemical shifts. (b) Static ^{13}C spectrum of peptide-bound bicelles at 283 K. The bicelle is in the isotropic phase at this temperature; thus, the chemical shifts are the same as in the MAS spectrum, but the line widths are broader. (c) Static ^{13}C spectrum of oriented bicelles without M2 at 300 K. The lipid chemical shifts differ from those in the MAS spectrum (a) because of the presence of CSA under the oriented condition. (d) Static ^{13}C spectrum of M2-bound oriented bicelles at 302 K. The peptide ^{13}C chemical shifts are slightly different from the isotropic shifts in spectra a and b because of the presence of CSA. Blue and red dashed lines guide the eye for chemical shift changes under different experimental conditions.

indicating that whole-body reorientation of the bicelle significantly scales the ^{13}C CSAs. The L26 Cβ and I35 Cδ1

DOI: 10.1021/acs.biochem.5b00127
Biochemistry 2015, 54, 2214−2226

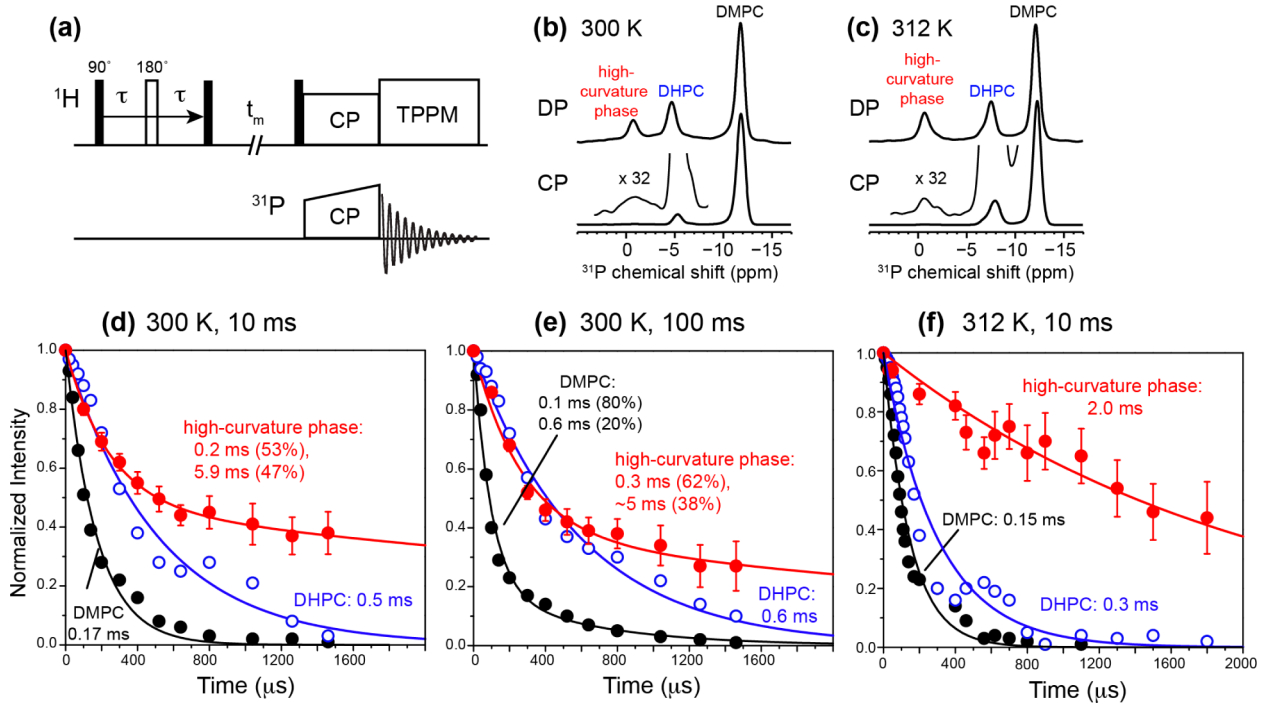

Figure 5. ^{31}P-detected ^{1}H T_2 relaxation data of DMPC/DHPC bicelles containing M2TM-AH under the static condition. (a) Pulse sequence of the indirectly detected ^{1}H T_2 experiment. (b) Representative ^{31}P DP and CP spectra with ^{1}H spin diffusion mixing at 300 K. (c) Representative ^{31}P DP and CP spectra with ^{1}H spin diffusion at 312 K. The ^{31}P chemical shifts differ between 300 and 312 K for DMPC and DHPC peaks because of temperature-dependent exchange of DHPC between the planar and edge regions of the bicelle. (d) ^{1}H T_2 relaxation decays at 300 K after 10 ms ^{1}H spin diffusion. (e) ^{1}H T_2 relaxation decays at 300 K after 100 ms ^{1}H spin diffusion. (f) ^{1}H T_2 relaxation decays at 312 K after 10 ms spin diffusion. The DMPC, DHPC, and high-curvature phase data are colored black, blue, and red, respectively.

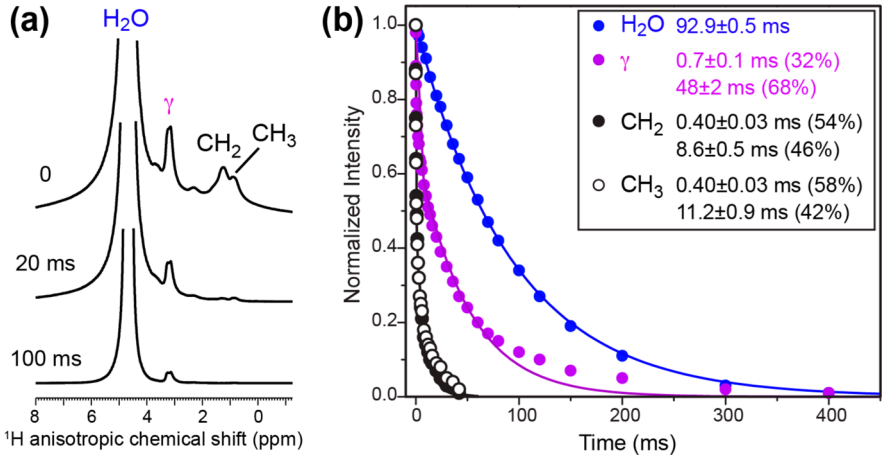

Figure 6. Directly detected ^{1}H T_2 relaxation data of DMPC/DHPC bicelles containing M2TM-AH under the static condition at 302 K. (a) Representative ^{1}H spectra with different echo delays. (b) ^{1}H T_2 relaxation curves with single- or double-exponential fits. The decay constants and the corresponding fractions are listed. The lipid relaxation times range from 0.4 to 50 ms, whereas the water ^{1}H T_2 relaxation time is much longer, 93 ms.

signals are particularly unambiguous and well-resolved; thus, they serve as probes of M2 partitioning in mixed-curvature membranes. To verify that the TM domain retains the same α-helical conformation in bicelles as in multilamellar liposomes, we measured a double-quantum-filtered ^{13}C spectrum of the sample, where the natural-abundance lipid ^{13}C signals are suppressed (Figure S2 of the Supporting Information). The spectrum shows the same α-helical chemical shifts for the labeled residues as reported before for multilamellar liposome samples.[32,44]

^{1}H T_2 Relaxation Times Indicate Preferential Localization of M2TM-AH in the High-Curvature Membrane. With resolved lipid and peptide ^{13}C signals in the static spectra of the oriented bicelles, we can measure the ^{1}H T_2 relaxation times of lipids with ^{31}P and ^{13}C detection (Figure 5a). ^{31}P detection allows us to investigate the dynamics of DMPC, DHPC, and the high-curvature lipids, while ^{13}C detection allows us to detect the dynamics of lipids in the vicinity of the peptide, thus revealing the membrane environment in which M2 resides.[13]

Figure 5 shows ^{31}P-detected ^{1}H T_2 relaxation data and representative ^{31}P spectra. We measured the ^{1}H T_2 at 300 K using 10 and 100 ms mixing to probe the dynamics of lipids in small and large domains. Among the three resolved membrane

DOI: 10.1021/acs.biochem.5b00127
Biochemistry 2015, 54, 2214−2226

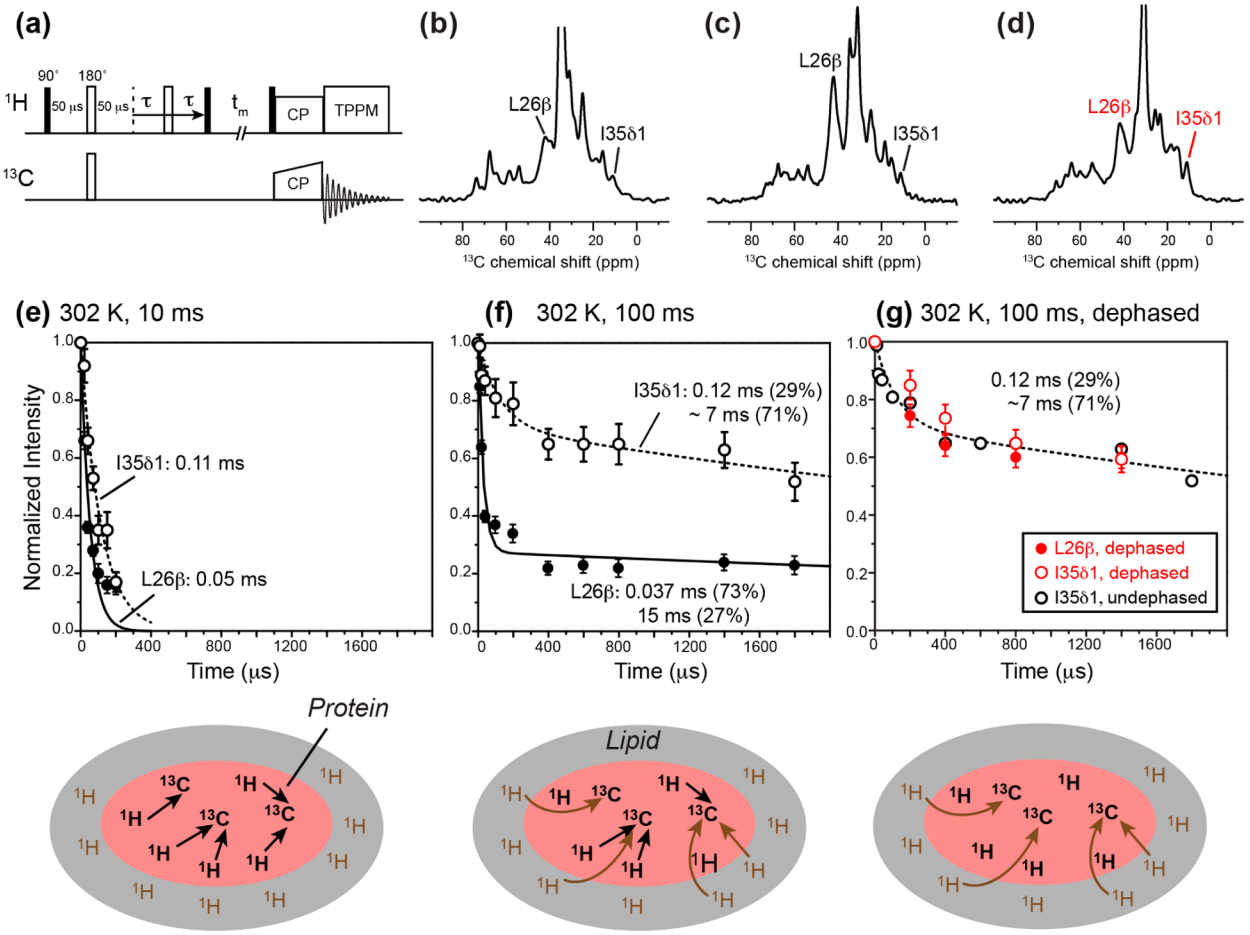

Figure 7. ^{13}C-detected ^{1}H T_2 relaxation data of M2TM-AH in oriented bicelles at 302 K under the static condition. (a) Pulse sequence of the dipolar-dephased ^{1}H T_2 relaxation experiment used to obtain the data in panel g. (b) Representative ^{13}C spectra without dipolar dephasing, measured with 10 ms ^{1}H spin diffusion. (c) Representative ^{13}C spectra without dipolar dephasing, measured with 100 ms ^{1}H spin diffusion. (d) Representative ^{13}C spectra with dipolar dephasing and 100 ms ^{1}H spin diffusion. The echo delay is 0 for all the spectra in panels b–d. (e) ^{13}C-detected ^{1}H T_2 relaxation curves with 10 ms spin diffusion. The schematic illustration below indicates that ^{1}H magnetization transfer is mostly within the peptide at this mixing time. (f) ^{13}C-detected ^{1}H T_2 relaxation curves after 100 ms spin diffusion. At this mixing time, lipid ^{1}H magnetization from the surrounding environment is transferred to the peptide, thus giving much slower relaxation. A fast initial decay is especially pronounced for the L26 Cβ signal. (g) ^{1}H T_2 relaxation curves measured with 100 μs C–H dipolar dephasing and 100 ms spin diffusion, to selectively detect the T_2 relaxation of lipids near the peptide. The disappearance of the fast initial decay of the L26 Cβ data verifies that the origin of the fast initial decay is the rigid peptide protons.

phases, DMPC undergoes the fastest relaxation with a ^{1}H T_2 of 0.1–0.2 ms, while the high-curvature phase has the slowest relaxation: apart from an initial decay of 0.1–0.2 ms, 40–50% of the intensity exhibits a T_2 of 5–6 ms (Figure 5d,e). The bicelle edge DHPC lipids exhibit an intermediate ^{1}H T_2 of ~0.5 ms. The slow relaxation of the high-curvature phase is understandable, because the lipids in this phase undergo not only uniaxial rotational diffusion around the local membrane normal but also isotropic tumbling and lateral diffusion over the highly curved membrane surface. Increasing the mixing time from 10 to 100 ms did not change the relaxation rates of DMPC and DHPC but increased the relaxation rates of the high-curvature phase, and the initial decay now overlaps with the initial DHPC decay. This convergence is in good agreement with the observed ^{31}P cross-peak between DHPC and the high-curvature lipids, further indicating that the high-curvature phase is associated with the bicelle edge DHPC lipids.

Increasing the temperature to 312 K brought interesting counterdirectional changes to the relaxation rates of DHPC and the high-curvature lipids: the high-curvature lipids relaxed more slowly, whereas the DHPC relaxation rates increased. The former indicates faster reorientations of the high-curvature lipids at high temperature, while the latter can be attributed to increased diffusion of DHPC between the planar and edge regions of the bicelle. The upfield ^{31}P chemical shift of −7.6 ppm at 312 K, compared to the value of −4.8 ppm at 300 K, is consistent with this increased level of exchange.

To determine whether the indirectly measured ^{1}H relaxation times of lipids differ from the directly measured values, we measured the T_2 of bicelles containing M2TM-AH by direct ^{1}H detection (Figure 6a). The acyl-chain CH_2 and CH_3 signals and the headgroup Hγ peak all exhibit biexponential decays, with a fast component of 0.4–0.7 ms and a slow component of ~10 ms for the chain protons and ~50 ms for the headgroup trimethylamine. For acyl-chain protons, we assign the short T_2 component to the oriented bicelle phase and the long T_2 to the dynamic high-curvature phase. The long-component T_2 values are larger than the T_2 values measured by ^{31}P detection, likely because direct detection favors the signals of highly dynamic protons while indirect detection by ^{1}H–^{31}P CP preferentially

DOI: 10.1021/acs.biochem.5b00127
Biochemistry 2015, 54, 2214–2226

enhances the signals of the more immobile protons. Compared to the lipid ^{1}H T_2 values, the water T_2 is much longer, ~93 ms, consistent with the presence of bulk water in these highly hydrated (65 wt %) samples.

Switching to ^{13}C detection for the ^{1}H T_2 measurement allowed us to probe the dynamics of lipids in the vicinity of M2TM-AH. At 302 K and with a short spin diffusion time of 10 ms, fast T_2 relaxation times of 50−110 μs were observed, indicating that only the relatively immobile peptide protons were detected (Figure 7e). Increasing the mixing time to 100 ms dramatically slowed the T_2 relaxation: both I35 and L26 side chains now exhibit biexponential decays with slow components of 7 and 15 ms, respectively (Figure 7f). The initial fast decay is dominant for the L26 Cβ signal and accounts for ~30% of the I35 Cδ1 signal. To verify that this initial fast decay results from peptide protons instead of an immobile pool of lipids, we added a ^{13}C−^{1}H dipolar filter of 100 μs before the echo period (Figure 7a and Figure S3 of the Supporting Information) to suppress the signals of the rigid peptide. Because the lipids are not ^{13}C-labeled, the dipolar filter does not impact the lipid signals. Figure 7g shows that this dipolar filter removed most of the fast initial decay and dramatically increased the L26 Cβ intensity, thus confirming that the lipids near the peptide have long ^{1}H T_2 relaxation times of ~7 ms. This T_2 value is closest to the ^{31}P-detected ^{1}H T_2 of the high-curvature lipids, but an order of magnitude longer than the relaxation times of bicelle lipids. Therefore, these ^{13}C- and ^{31}P-detected ^{1}H T_2 data indicate that M2TM-AH is preferentially bound to the high-curvature domain.

OMAS 2D ^{1}H−^{31}P Correlation NMR for Detecting M2(21−61) Partitioning in Bicelles. We measured 2D ^{31}P−^{1}H correlation spectra to detect lipid ^{31}P−protein H^N correlation signals directly. Although the ^{31}P signals of the three membrane components are well-resolved under the static condition, the collective protein H^N signals are expected to be much broader than the lipid ^{1}H signals under the static oriented condition, because membrane-bound proteins usually exhibit greater orientational disorder and slower motional rates than lipids, thus giving rise to larger residual ^{1}H−^{1}H dipolar couplings. Therefore, we chose to spin the bicelle to obtain the necessary sensitivity and resolution. Because all three lipid components have the same ^{31}P isotropic chemical shift, they are unresolved in the ^{31}P MAS spectrum (Figure 8a), making it necessary to conduct OMAS experiments. Deviating from the magic angle by a small degree already led to sufficient ^{31}P CSAs and site resolution while retaining reasonable ^{1}H line width. In the spectrum shown in Figure 8b, all three lipid signals are resolved and readily assigned on the basis of their relative intensities and the effective ^{31}P CSAs. The most downfield and highest peak can be assigned to DMPC, while the most upfield and weakest peak can be assigned to the high-curvature membrane domain. Changing the sample axis to the other side of the magic angle caused the opposite frequency changes, with DMPC giving the most upfield chemical shift (Figure 8c).

The precise angles (θ) of the rotation axis from the magnetic field can be determined from the chemical shift differences among the ^{31}P MAS, OMAS, and static spectra. The static spectrum in Figure 8d is equivalent to a θ = 0° OMAS spectrum with a scaling factor $(3\cos^2\theta - 1)/2$ of 1. The OMAS spectrum of Figure 8b has an intensity distribution opposite from that of the static spectrum, indicating that the rotation axis is tilted by an angle larger than 54.7° to cause a negative scaling factor to the ^{31}P CSA. The DMPC ^{31}P

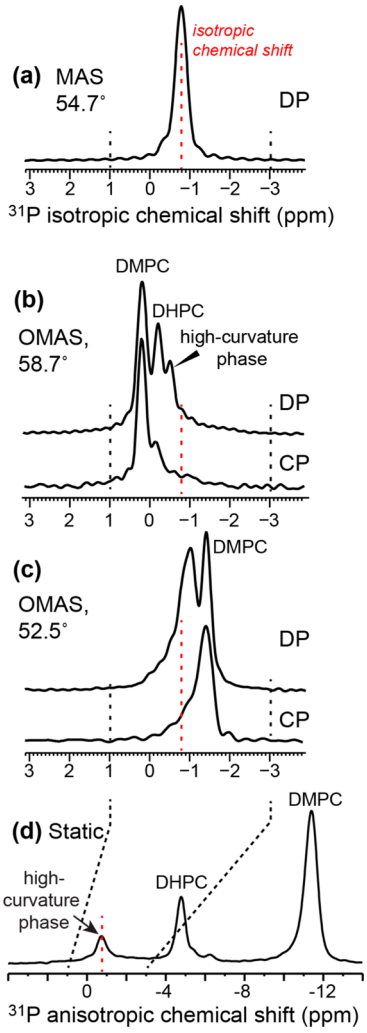

Figure 8. One-dimensional ^{31}P spectra of bicelles containing M2TM-AH under 3.5 kHz spinning at 300 K. (a) ^{31}P DP MAS spectrum. (b) ^{31}P DP and CP spectra under OMAS at 58.7°. Three ^{31}P peaks are resolved. (c) ^{31}P DP and CP spectra under OMAS at 52.5°. (d) Comparative static ^{31}P spectrum, showing three well-resolved peaks.

chemical shift is 1.0 ppm larger than the isotropic chemical shift in Figure 8b but 10.6 ppm smaller than the isotropic frequency in the static spectrum (Figure 8d). Thus, the scaling factor is 1/(−10.6) = −0.094, which corresponds to a rotation angle of 58.7°. Similar arguments indicate a rotation angle of 52.5° for the spectrum in Figure 8c.

Figure 9 shows the 2D ^{1}H−^{31}P correlation spectra of DMPC/DHPC bicelles containing M2TM-AH under 58.7° OMAS. Without ^{1}H spin diffusion, the DMPC and DHPC ^{31}P signals correlate with only lipid protons such as glycerol G2 (5.4 ppm) and G3 and headgroup α/β (4.2 ppm) (Figure 9b). These anisotropic ^{1}H chemical shifts do not deviate significantly from the isotropic values measured in the MAS spectrum (Figure 9d,e) because of the small motionally averaged ^{1}H CSAs and the small deviation of the rotation angle from the magic angle. With 0.5 ms ^{1}H spin diffusion, ^{31}P−lipid-chain ^{1}H cross-peaks were observed. Importantly, broad H^N signals at 6−9 ppm are seen to correlate with the DMPC ^{31}P peak but not the DHPC peak (Figure 9c,f), indicating that some M2TM-AH partitions into the planar region of the bicelles. The amide protons that correlate with the

DOI: 10.1021/acs.biochem.5b00127
Biochemistry 2015, 54, 2214−2226

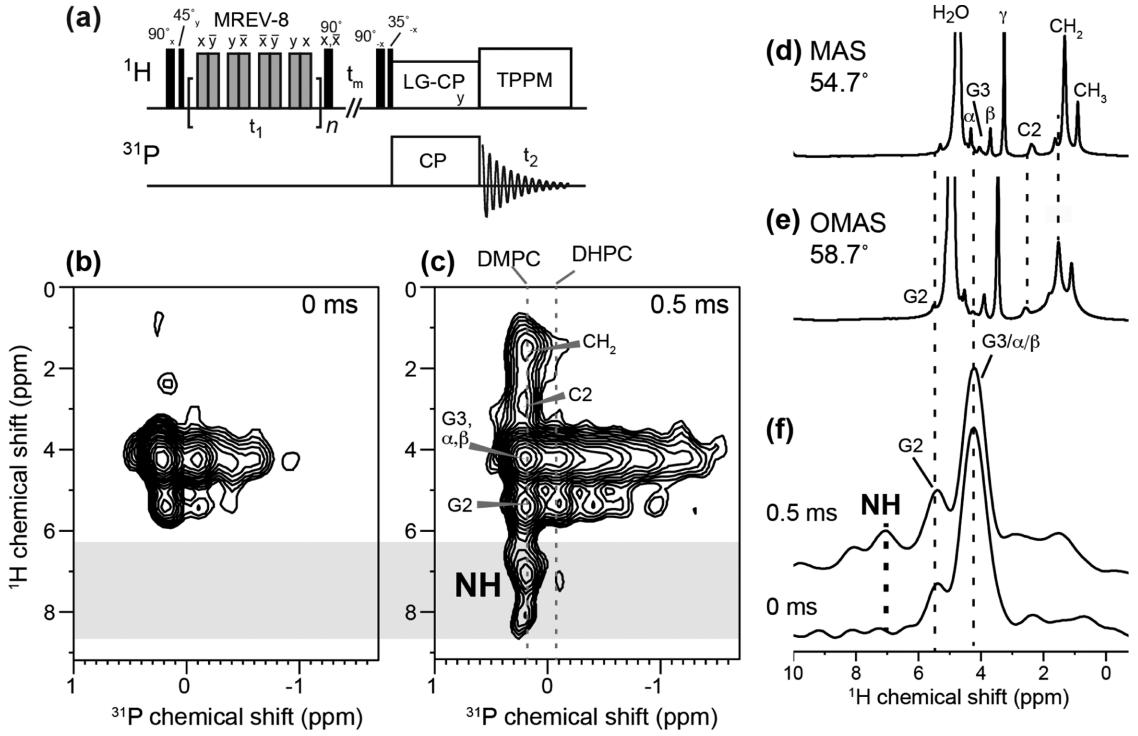

Figure 9. 2D $^{31}P-^{1}H$ correlation spectra with ^{1}H homonuclear decoupling, measured at 306 K under OMAS at 58.7°. (a) Pulse sequence for the homonuclear-decoupled HETCOR experiment. (b) 2D spectrum without ^{1}H spin diffusion. (c) 2D spectrum with 0.5 ms ^{1}H spin diffusion. (d) One-dimensional ^{1}H MAS spectrum. (e) One-dimensional ^{1}H OMAS spectrum at 58.7°. (f) ^{1}H cross sections of DMPC with 0.5 ms (top) and 0 ms (bottom) spin diffusion, extracted from the 2D spectra in panels b and c.

DMPC ^{31}P most likely result from the surface-bound amphipathic helix rather than the TM domain.[45]

Taken together, the one-dimensional ^{31}P and ^{2}H spectra and the 2D $^{31}P-^{31}P$ exchange spectra show that the M2 amphipathic helix generates a high-curvature membrane domain that is associated with the DHPC edges of bicelles, while ^{1}H relaxation data and 2D $^{1}H-^{31}P$ correlation spectra indicate that the protein predominantly binds the high-curvature domain, followed by a small fraction that partitions into the planar region of the bicelle. These results are depicted in Figure 10, where the high-curvature phase is represented as micelles, although a bicontinuous cubic phase cannot be ruled out.

DISCUSSION

So far, bicelles have been mainly used to determine the high-resolution structures of membrane proteins by solution and solid-state NMR spectroscopy.[46−49] The data shown here represent a novel application of bicelles as a medium for characterizing protein-induced membrane curvature. The static ^{31}P spectra distinguish the lipid signals in the planar and edge regions of the bicelle from lipids in high-curvature phases. By comparing ^{31}P-detected and ^{13}C-detected lipid ^{1}H relaxation times, we can deduce the dynamic and curvature environment of the protein. By correlating lipid ^{31}P and protein ^{1}H chemical shifts, we can further define the protein binding sites.

The fact that M2(21−61) and not M2(22−46) generates the isotropic ^{31}P chemical shift and a zero-frequency ^{2}H peak in the static spectra indicates that the amphipathic helix is solely responsible for incurring membrane curvature. The high-curvature phase can be micelles, small vesicles, or bicontinuous cubic phases, all of which possess the symmetry to give an

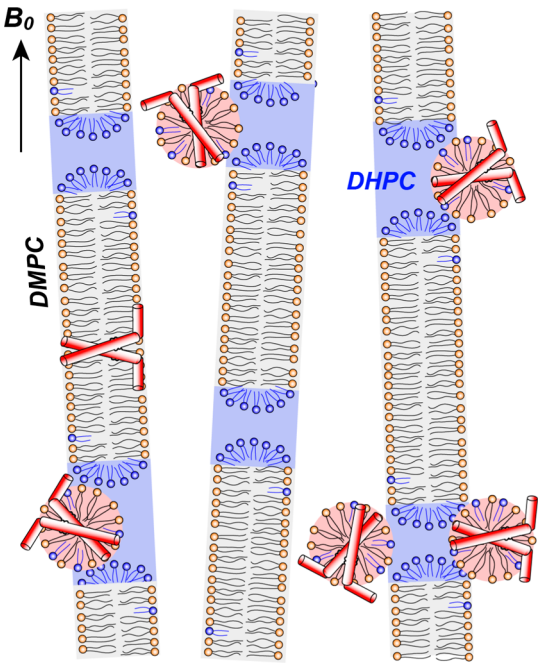

Figure 10. Schematic of M2TM-AH binding to membranes with mixed curvatures. The peptide creates a high-curvature phase that is partially associated with the round caps of bicelles. Depicted here are micelles, but bicontinuous cubic phases cannot be ruled out. Most of the peptide binds to this high-curvature phase, while a small fraction resides in the planar region of the bicelle because of its stabilization of the hydrophobic TM helix. For simplicity, only two of the four molecules of the tetrameric protein are represented.

DOI: 10.1021/acs.biochem.5b00127
Biochemistry 2015, 54, 2214−2226

isotropic NMR peak. Recent synchrotron SAXS data indicate that both full-length M2 and an M2 peptide encompassing the TM and AH domains generate bicontinuous cubic phases.[7] Full-length M2 required >60 mol % phosphatidylethanolamine (PE) in the membrane to induce the cubic phase, and the SAXS spectra index to an *Ia*3*d* gyroid phase with lattice parameters of ∼20 nm. The TM-AH peptide generated a mixture of *Pn*3*m* and *Im*3*m* phases over a wider range of lipid compositions. In PE-free DOPC/DOPS membranes, a *Pn*3*m* double-diamond phase was observed with lattice parameters of 21−29 nm. These bicontinuous cubic phases have the common characteristics of negative Gaussian curvature, which is the type of curvature present in the neck of a budding virus. Thus, their generation by the AH-containing M2 protein is consistent with the membrane scission function of M2.[6] Although it is tempting to conclude, on the basis of these SAXS data, that the isotropic ^{31}P and ^{2}H peaks detected here also result from a cubic phase, several factors argue for a micellar interpretation. DMPC and DHPC lipids have significantly stronger positive intrinsic curvature than that of the unsaturated DOPC, DOPS, and DOPE lipids used in the SAXS study; thus, a micellar phase with positive curvature is possible. From a biological standpoint, while the bicontinuous cubic phase captures the membrane geometry at the neck of the budding virus,[6] the micelle morphology captures the membrane curvature of the virus away from the budding neck. Finally, the exchange peak between DHPC and the isotropic peak in the 2D ^{31}P−^{31}P correlation spectra indicates that the high-curvature phase is partly associated with the bicelle edges (Figure 3). Bicontinuous phases have much larger overall dimensions because of their periodically repeating nature,[50,51] thus they are less likely to form significant contacts with other membrane phases. Thus, the ^{31}P cross-peak in the 2D spectra is also in favor of a micellar interpretation of the isotropic peak in the ^{31}P and ^{2}H NMR spectra.

Because the high-curvature phase generated by M2TM-AH represents only a small fraction (10−20%) of all lipids in our samples, preferential binding of M2 to this domain may seem counterintuitive. However, equilibrium consideration indicates that this preferential binding is to be expected, because if the protein resides only in the low-curvature membrane while inducing high-curvature domains, the lamellar domain will eventually be depleted. Therefore, the small fraction of the high-curvature domain must be enriched with the protein at equilibrium. Given the preference of M2TM-AH for the high-curvature phase, a natural question is why a small amount of M2 binds the planar DMPC region rather than the round DHPC edges of the bicelle. We attribute this result to the unfavorable geometry of the bicelle edges. For the amphipathic helix to lie on the round caps formed by DHPC, the TM helix must lie perpendicular to the interior DMPC chains. This orientation is not only sterically unfavorable but also prevents the exposure of the N-terminus of the TM helix to water, which is seen in all high-resolution structures of M2.[27,30,45,52] In contrast, M2 binding to the planar DMPC region of the bicelle satisfies hydrophobic interactions of the TM helix with the membrane as well as polar interactions of the terminal residues with water and is thus energetically favorable. On the basis of the ^{13}C-detected ^{1}H T_2 relaxation data (Figure 7f), we estimate that ∼70% of M2TM-AH binds the high-curvature domain while ∼30% binds the lamellar domain.

Several mechanisms exist with which proteins can induce high membrane curvature. First, amphipathic helices in proteins can insert asymmetrically into one leaflet of the membrane to promote local curvature. An example is the fusion peptide of the influenza hemagglutinin.[4,53] Analogously, integral membrane proteins or protein assemblies with intrinsic curvature can induce membrane curvature by inserting into the membrane. Second, peripheral membrane proteins can brace the lipid bilayer like a scaffold to deform them into nonlamellar morphologies. For example, the dynamin family of proteins can bend the membrane into tubules to mediate vesicle invagination, membrane scission, and cell division.[1] Third, arginine-rich peptides such as antimicrobial peptides and cell-penetrating peptides can induce membrane curvature by electrostatic interactions between the cationic residues and lipid phosphates.[12,40,54−57] The M2 amphipathic helix, which lies on the membrane surface,[45] likely induces membrane curvature through the scaffolding mechanism.

The fact that M2TM-AH generates a high-curvature phase to the simple DMPC/DHPC membrane, without cholesterol, is noteworthy. A previous study of M2TM-AH in a virus-mimetic membrane containing phosphocholine, phosphoethanolamine, sphingomyelin, and cholesterol also detected a ^{31}P isotropic peak.[13] Combined with the recent SAXS results, which were obtained in cholesterol-free membranes,[7] these biophysical data together document that M2TM-AH can generate curvature in a variety of membrane compositions, and cholesterol is not a necessary condition for curvature induction. However, the exact type of curvature may differ among different membrane compositions, because the lipid components may affect the depth of the amphipathic helix, the clustering of the M2 tetramers, and the orientation of the TM and amphipathic helices.[45,58−60] Additional experiments will be necessary to determine the types of membrane curvature induced by M2 in various lipid environments.

The 2D OMAS correlation NMR experiment shown here is analogous to variable-angle spinning, switched-angle spinning, and dynamic-angle spinning experiments pioneered by Terao, Pines, and Fung.[61−65] Most of these techniques focused on separating anisotropic interactions such as dipolar couplings and quadrupolar couplings in the indirect dimension by isotropic chemical shifts in the direct dimension. The current experiment differs in using anisotropic chemical shifts to resolve different membrane curvatures rather than chemical functional groups. Interestingly, the rotation angle determined from our ^{31}P spectra (Figure 8) under 3.5 kHz spinning indicates a different bicelle alignment from that predicted by the classical theory of variable-angle spinning of liquid crystals.[66] The classical theory states that when the spinning frequency is larger than a critical frequency of several hundred hertz, liquid crystals do not have time to align with the magnetic field and adopt an orientation that minimizes the time-averaged potential energy. For liquid crystals with a negative anisotropy of magnetic susceptibility, $\Delta\chi$, which is the case for bicelles, the bilayer directors are predicted to be distributed in a plane perpendicular to the rotation axis ($\beta = 90°$) when rotation angle θ is smaller than the magic angle, but the directors would be parallel to the rotation axis ($\beta = 0°$) when $\theta > 54.7°$.[67,68] The overall scaling factor, $(3\cos^2\theta - 1)/2 \times (3\cos^2\beta - 1)/2$, is therefore negative under both conditions, indicating that the anisotropic ^{31}P chemical shift should be smaller than the isotropic shift at all rotation angles. This was observed for spinning frequencies of <1 kHz,[35,69] but under our spinning frequency of 3.5 kHz, the spectrum in Figure 8b shows ^{31}P chemical shifts that are larger than (i.e., downfield from) the

DOI: 10.1021/acs.biochem.5b00127
Biochemistry 2015, 54, 2214−2226

isotropic chemical shift, which translates to a positive overall scaling factor. This indicates that the directors remain perpendicular to the rotation axis even when $\theta > 54.7°$, in contrast to the classical theory. This bicelle orientation under fast spinning has also been reported by Meier and co-workers[35] and suggests that under fast spinning, the directors do not have time to change their alignment axis from the nonspinning condition and instead remain perpendicular to the rotation axis.

A relatively high amide H^N chemical shift resolution of ~0.4 ppm on bicelle-bound membrane proteins has recently been shown to be achievable under the static condition, without spinning, by using optimized $^1H-^1H$ homonuclear decoupling sequences and by correlating H^N chemical shifts with ^{15}N chemical shifts.[70,71] The OMAS $^1H-^{31}P$ correlation technique is complementary to that approach. Because $H^N-^{31}P$ cross-peaks are intermolecular by design, all protein amide H^N signals are observed together in the same ^{31}P cross section; thus, residue-specific H^N resolution is not necessary in our experiment. In addition, surface-bound membrane protein domains such as the M2 amphipathic helix may be less uniformly oriented than transmembrane segments; thus, the OMAS approach, which is independent of the degree of alignment, is more robust for these difficult-to-orient membrane proteins.

CONCLUSION

We presented two bicelle-based SSNMR methods for determining membrane curvature and the binding site of proteins in mixed-curvature membranes. We demonstrated these methods on the influenza M2 protein, which mediates membrane scission during virus budding in addition to serving as a proton channel for virus uncoating. Our data show that the amphipathic helix in M2 confers the ability to cause high membrane curvature and directs the protein to this high-curvature domain, while a small fraction of the protein resides in the planar region of the bicelle. The M2-induced high-curvature phase is associated with the round edges of the bicelles, reminiscent of the membrane geometry and deformation in a budding virus. The indirectly detected of the lipid ^1H relaxation NMR experiment and the 2D OMAS heteronuclear correlation technique are generally applicable to a wide range of membrane proteins for determining their binding sites in complex membranes with multiple curvatures.

ASSOCIATED CONTENT

Supporting Information

Additional NMR spectra. This material is available free of charge via the Internet at http://pubs.acs.org.

AUTHOR INFORMATION

Corresponding Author

*E-mail: meihong@mit.edu.

Funding

This work is supported by National Institutes of Health Grant GM088204 to M.H.

Notes

The authors declare no competing financial interest.

REFERENCES

(1) McMahon, H. T., and Gallop, J. L. (2005) Membrane curvature and mechanisms of dynamic cell membrane remodelling. *Nature 438*, 590−596.

(2) Mim, C., and Unger, V. M. (2012) Membrane curvature and its generation by BAR proteins. *Trends Biochem. Sci. 37*, 526−533.

(3) Harrison, S. C. (2008) Viral membrane fusion. *Nat. Struct. Mol. Biol. 15*, 690−698.

(4) Han, X., Bushweller, J. H., Cafiso, D. S., and Tamm, L. K. (2001) Membrane structure and fusion-triggering conformational change of the fusion domain from influenza hemagglutinin. *Nat. Struct. Biol. 8*, 715−720.

(5) Yao, H., and Hong, M. (2014) Conformation and lipid interaction of the fusion peptide of the paramyxovirus PIV5 in anionic and negative-curvature membranes from solid-state NMR. *J. Am. Chem. Soc. 136*, 2611−2624.

(6) Rossman, J. S., Jing, X., Leser, G. P., and Lamb, R. A. (2010) Influenza virus M2 protein mediates ESCRT-independent membrane scission. *Cell 142*, 902−913.

(7) Schmidt, N. W., Mishra, A., Wang, J., DeGrado, W. F., and Wong, G. C. (2013) Influenza virus A M2 protein generates negative Gaussian membrane curvature necessary for budding and scission. *J. Am. Chem. Soc. 135*, 13710−13719.

(8) Gidalevitz, D., Ishitsuka, Y., Muresan, A. S., Konovalov, O., Waring, A. J., Lehrer, R. I., and Lee, K. Y. (2003) Interaction of antimicrobial peptide protegrin with biomembranes. *Proc. Natl. Acad. Sci. U.S.A. 100*, 6302−6307.

(9) Mishra, A., Gordon, V. D., Yang, L., Coridan, R., and Wong, G. C. (2008) HIV TAT forms pores in membranes by inducing saddle-splay curvature: Potential role of bidentate hydrogen bonding. *Angew. Chem., Int. Ed. 47*, 2986−2989.

(10) Wang, T., Yao, H., and Hong, M. (2013) Determining the depth of insertion of dynamically invisible membrane peptides by gel-phase ^1H spin diffusion heteronuclear correlation NMR. *J. Biomol. NMR 56*, 139−148.

(11) Huster, D., Yao, X., and Hong, M. (2002) Membrane protein topology probed by ^1H spin diffusion from lipids using solid-state NMR spectroscopy. *J. Am. Chem. Soc. 124*, 874−883.

(12) Mani, R., Cady, S. D., Tang, M., Waring, A. J., Lehrer, R. I., and Hong, M. (2006) Membrane-dependent oligomeric structure and pore formation of a β-hairpin antimicrobial peptide in lipid bilayers from solid-state NMR. *Proc. Natl. Acad. Sci. U.S.A. 103*, 16242−16247.

(13) Wang, T., Cady, S. D., and Hong, M. (2012) NMR determination of protein partitioning into membrane domains with different curvatures and application to the influenza M2 peptide. *Biophys. J. 102*, 787−794.

(14) Sanders, C. R., and Landis, G. C. (1995) Reconstitution of membrane proteins into lipid-rich bilayered mixed micelles for NMR studies. *Biochemistry 34*, 4030−4040.

(15) Sanders, C. R., and Schwonek, J. P. (1992) Characterization of magnetically orientable bilayers in mixtures of dihexanoylphosphatidylcholine and dimyristoylphosphatidylcholine by solid-state NMR. *Biochemistry 31*, 8898−8905.

(16) Sanders, C. R., Hare, B. J., Howard, K. P., and Prestegard, J. H. (1994) Magnetically-oriented phospholipid micelles as a tool for the study of membrane-associated molecules. *Prog. Nucl. Magn. Reson. Spectrosc. 26*, 421−444.

(17) Ottiger, M., and Bax, A. (1998) Characterization of magnetically oriented phospholipid micelles for measurement of dipolar couplings in macromolecules. *J. Biomol. NMR 12*, 361−372.

(18) Tolman, J. R., Al-Hashimi, H. M., Kay, L. E., and Prestegard, J. H. (2001) Structural and dynamic analysis of residual dipolar coupling data for proteins. *J. Am. Chem. Soc. 123*, 1416−1424.

(19) Prosser, R. S., Evanics, F., Kitevski, J. L., and Al-Abdul-Wahid, M. S. (2006) Current applications of bicelles in NMR studies of membrane-associated amphiphiles and proteins. *Biochemistry 45*, 8453−8465.

(20) Prosser, R. S., Hunt, S. A., DiNatale, J. A., and Vold, R. R. (1996) Magnetically aligned membrane model systems with positive order parameter: Switching the sign of S-zz with paramagnetic ions. *J. Am. Chem. Soc. 118*, 269−270.

DOI: 10.1021/acs.biochem.5b00127
Biochemistry 2015, 54, 2214−2226

(21) Tan, C. B., Fung, B. M., and Cho, G. J. (2002) Phospholipid bicelles that align with their normals parallel to the magnetic field. *J. Am. Chem. Soc. 124*, 11827−11832.
(22) Glover, K. J., Whiles, J. A., Wu, G., Yu, N., Deems, R., Struppe, J. O., Stark, R. E., Komives, E. A., and Vold, R. R. (2001) Structural evaluation of phospholipid bicelles for solution-state studies of membrane-associated biomolecules. *Biophys. J. 81*, 2163−2171.
(23) Gaemers, S., and Bax, A. (2001) Morphology of three lyotropic liquid crystalline biological NMR media studied by translational diffusion anisotropy. *J. Am. Chem. Soc. 123*, 12343−12352.
(24) Nieh, M. P., Raghunathan, V. A., Glinka, C. J., Harroun, T. A., Pabst, G., and Katsaras, J. (2004) Magnetically alignable phase of phospholipid "bicelle" mixtures is a chiral nematic made up of wormlike micelles. *Langmuir 20*, 7893−7897.
(25) Triba, M. N., Warschawski, D. E., and Devaux, P. F. (2005) Reinvestigation by phosphorus NMR of lipid distribution in bicelles. *Biophys. J. 88*, 1887−1901.
(26) Pinto, L. H., Holsinger, L. J., and Lamb, R. A. (1992) Influenza virus M2 protein has ion channel activity. *Cell 69*, 517−528.
(27) Cady, S. D., Schmidt-Rohr, K., Wang, J., Soto, C. S., Degrado, W. F., and Hong, M. (2010) Structure of the amantadine binding site of influenza M2 proton channels in lipid bilayers. *Nature 463*, 689−692.
(28) Cady, S., Wang, T., and Hong, M. (2011) Membrane-dependent effects of a cytoplasmic helix on the structure and drug binding of the influenza virus M2 protein. *J. Am. Chem. Soc. 133*, 11572−11579.
(29) Jing, X., Ma, C., Ohigashi, Y., Oliveira, F. A., Jardetzky, T. S., Pinto, L. H., and Lamb, R. A. (2008) Functional studies indicate amantadine binds to the pore of the influenza A virus M2 proton-selective ion channel. *Proc. Natl. Acad. Sci. U.S.A. 105*, 10967−10972.
(30) Stouffer, A. L., Acharya, R., Salom, D., Levine, A. S., Di Costanzo, L., Soto, C. S., Tereshko, V., Nanda, V., Stayrook, S., and DeGrado, W. F. (2008) Structural basis for the function and inhibition of an influenza virus proton channel. *Nature 451*, 596−599.
(31) Hong, M., and Degrado, W. F. (2012) Structural basis for proton conduction and inhibition by the influenza M2 protein. *Protein Sci. 21*, 1620−1633.
(32) Cady, S. D., Mishanina, T. V., and Hong, M. (2009) Structure of amantadine-bound M2 transmembrane peptide of influenza A in lipid bilayers from magic-angle-spinning solid-state NMR: The role of Ser31 in amantadine binding. *J. Mol. Biol. 385*, 1127−1141.
(33) De Angelis, A. A., and Opella, S. J. (2007) Bicelle samples for solid-state NMR of membrane proteins. *Nat. Protoc. 2*, 2332−2338.
(34) Williams, J. K., and Hong, M. (2014) Probing membrane protein structure using water polarization transfer solid-state NMR. *J. Magn. Reson. 247*, 118−127.
(35) Zandomeneghi, G., Tomaselli, M., Williamson, P. T., and Meier, B. H. (2003) NMR of bicelles: Orientation and mosaic spread of the liquid-crystal director under sample rotation. *J. Biomol. NMR 25*, 113−123.
(36) Rhim, W.-K., Elleman, D. D., and Vaughan, R. W. (1973) Analysis of multiple-pulse NMR in solids. *J. Chem. Phys. 59*, 3740−3749.
(37) Li, S., Su, Y., Luo, W., and Hong, M. (2010) Water-protein interactions of an arginine-rich membrane peptide in lipid bilayers investigated by solid-state nuclear magnetic resonance spectroscopy. *J. Phys. Chem. B 114*, 4063−4069.
(38) Triba, M. N., Devaux, P. F., and Warschawski, D. E. (2006) Effects of lipid chain length and unsaturation on bicelles stability. A phosphorus NMR study. *Biophys. J. 91*, 1357−1367.
(39) Sternin, E., Nizza, D., and Gawrisch, K. (2001) Temperature Dependence of DMPC/DHPC Mixing in a Bicellar Solution and Its Structural Implications. *Langmuir 17*, 2610−2616.
(40) Tang, M., Waring, A. J., and Hong, M. (2007) Trehalose-protected lipid membranes for determining membrane protein structure and insertion. *J. Magn. Reson. 184*, 222−227.
(41) Marasinghe, P. A. B., Buffy, J. J., Schmidt-Rohr, K., and Hong, M. (2005) Membrane curvature change induced by an antimicrobial peptide detected by ^{31}P exchange NMR. *J. Phys. Chem. B 109*, 22036−22044.
(42) Saleem, Q., Lai, A., Morales, H. H., and Macdonald, P. M. (2012) Lateral diffusion of bilayer lipids measured via ^{31}P CODEX NMR. *Chem. Phys. Lipids 165*, 721−730.
(43) Lee, M., and Hong, M. (2014) Cryoprotection of lipid membranes for high-resolution solid-state NMR studies of membrane peptides and proteins at low temperature. *J. Biomol. NMR 59*, 263−277.
(44) Cady, S. D., Goodman, C., Tatko, C., DeGrado, W. F., and Hong, M. (2007) Determining the orientation of uniaxially rotating membrane proteins using unoriented samples: A ^{2}H, ^{13}C, and ^{15}N solid-state NMR investigation of the dynamics and orientation of a transmembrane helical bundle. *J. Am. Chem. Soc. 129*, 5719−5729.
(45) Sharma, M., Yi, M., Dong, H., Qin, H., Peterson, E., Busath, D., Zhou, H. X., and Cross, T. A. (2010) Insight into the mechanism of the influenza A proton channel from a structure in a lipid bilayer. *Science 330*, 509−512.
(46) Tjandra, N., and Bax, A. (1997) Direct measurement of distances and angles in biomolecules by NMR in a dilute liquid crystalline medium. *Science 278*, 1111−1114.
(47) Prosser, R. S., Evanics, F., Kitevski, J. L., and Al-Abdul-Wahid, M. S. (2006) Current applications of bicelles in NMR studies of membrane-associated amphiphiles and proteins. *Biochemistry 45*, 8453−8465.
(48) De Angelis, A. A., Howell, S. C., Nevzorov, A. A., and Opella, S. J. (2006) Structure determination of a membrane protein with two transmembrane helices in aligned phospholipid bicelles by solid-state NMR spectroscopy. *J. Am. Chem. Soc. 128*, 12256−12267.
(49) Xu, J., Durr, U. H., Im, S. C., Gan, Z., Waskell, L., and Ramamoorthy, A. (2008) Bicelle-enabled structural studies on a membrane-associated cytochrome B5 by solid-state MAS NMR spectroscopy. *Angew. Chem., Int. Ed. 47*, 7864−7867.
(50) Luzzati, V., and Spegt, P. A. (1967) Polymorphism of lipids. *Nature 215*, 701−704.
(51) Scriven, L. E. (1976) Equilibrium bicontinuous structure. *Nature 263*, 123−125.
(52) Schnell, J. R., and Chou, J. J. (2008) Structure and mechanism of the M2 proton channel of influenza A virus. *Nature 451*, 591−595.
(53) Tamm, L. K. (2003) Hypothesis: Spring-loaded boomerang mechanism of influenza hemagglutinin-mediated membrane fusion. *Biochim. Biophys. Acta 1614*, 14−23.
(54) Schmidt, N. W., Lis, M., Zhao, K., Lai, G. H., Alexandrova, A. N., Tew, G. N., and Wong, G. C. L. (2012) Molecular Basis for Nanoscopic Membrane Curvature Generation from Quantum Mechanical Models and Synthetic Transporter Sequences. *J. Am. Chem. Soc. 134*, 19207−19216.
(55) Schmidt, N. W., Mishra, A., Lai, G. H., Davis, M., Sanders, L. K., Tran, D., Garcia, A., Tai, K. P., McCray, P. B., Ouellette, A. J., Selsted, M. E., and Wong, G. C. (2011) Criterion for amino acid composition of defensins and antimicrobial peptides based on geometry of membrane destabilization. *J. Am. Chem. Soc. 133*, 6720−6727.
(56) Tang, M., and Hong, M. (2009) Structure and mechanism of β-hairpin antimicrobial peptides in lipid bilayers from solid-state NMR spectroscopy. *Mol. BioSyst. 5*, 317−322.
(57) Hong, M., and Su, Y. (2011) Structure and dynamics of cationic membrane peptides and proteins: Insights from solid-state NMR. *Protein Sci. 20*, 641−655.
(58) Hu, F., Luo, W., Cady, S. D., and Hong, M. (2011) Conformational plasticity of the influenza A M2 transmembrane peptide in lipid bilayers under varying pH, drug binding and membrane thickness. *Biochim. Biophys. Acta 1808*, 415−423.
(59) Luo, W., Cady, S. D., and Hong, M. (2009) Immobilization of the Influenza A M2 Transmembrane Peptide in Virus-Envelope Mimetic Lipid Membranes: A Solid-State NMR Investigation. *Biochemistry 48*, 6361−6368.
(60) Nguyen, P. A., Soto, C. S., Polishchuk, A., Caputo, G. A., Tatko, C. D., Ma, C., Ohigashi, Y., Pinto, L. H., DeGrado, W. F., and Howard,

DOI: 10.1021/acs.biochem.5b00127
Biochemistry 2015, 54, 2214−2226

K. P. (2008) pH-induced conformational change of the influenza M2 protein C-terminal domain. *Biochemistry 47*, 9934−9936.
(61) Terao, T., Miura, H., and Saika, A. (1986) I-S Dipolar Switching-Angle Spinning 2D NMR (SLF). *J. Chem. Phys. 85*, 3816−3826.
(62) Fung, B. M., and Afzal, J. (1986) C-13 NMR of liquid-crystals: Spinning near the magic angle with proton-proton dipolar decoupling. *J. Am. Chem. Soc. 108*, 1107−1108.
(63) Kolbert, A. C., Grandinetti, P. J., Baldwin, M., Pruisner, S. B., and Pines, A. (1994) Measurement of internuclear distances by switched angle spinning NMR. *J. Phys. Chem. 98*, 7936−7938.
(64) Mueller, K. T., Samoson, A., Sun, B. Q., Chingas, G. C., Zwanziger, J. W., Terao, T., and Pines, A. (1990) Dynamic-angle spinning of quadrupolar nuclei. *J. Magn. Reson. 86*, 470.
(65) Frydman, L., Chingas, G. C., Lee, Y. K., Grandinetti, P. J., Eastman, M. A., Barrall, G. A., and Pines, A. (1992) Variable-angle correlation spectroscopy in solid-state nuclear magnetic resonance. *J. Chem. Phys. 97*, 4800.
(66) Courtieu, J., Bayle, J. P., and Fung, B. M. (1994) Variable angle sample spinning NMR in liquid crystals. *Prog. Nucl. Magn. Reson. Spectrosc. 26*, 141−169.
(67) Hong, M., Pines, A., and Caldarelli, S. (1996) Measurement and Assignment of Long-Range C−H Dipolar Couplings in Liquid Crystals by Two-Dimensional NMR Spectroscopy. *J. Phys. Chem. 100*, 14815−14822.
(68) Caldarelli, S., Hong, M., Emsley, L., and Pines, A. (1996) Measurement of Carbon−Proton Dipolar Couplings in Liquid Crystals by Local Dipolar Field NMR Spectroscopy. *J. Phys. Chem. 100*, 18696−18701.
(69) Zandomeneghi, G., Williamson, P. T., Hunkeler, A., and Meier, B. H. (2003) Switched-angle spinning applied to bicelles containing phospholipid-associated peptides. *J. Biomol. NMR 25*, 125−132.
(70) Lu, G. J., and Opella, S. J. (2014) Resonance assignments of a membrane protein in phospholipid bilayers by combining multiple strategies of oriented sample solid-state NMR. *J. Biomol. NMR 58*, 69−81.
(71) Lu, G. J., Park, S. H., and Opella, S. J. (2012) Improved ^{1}H amide resonance line narrowing in oriented sample solid-state NMR of membrane proteins in phospholipid bilayers. *J. Magn. Reson. 220*, 54−61.

DOI: 10.1021/acs.biochem.5b00127
Biochemistry 2015, 54, 2214−2226

Supporting Information

Investigation of the Curvature Induction and Membrane Localization of the Influenza Virus M2 Protein Using Static and Off-Magic-Angle Spinning Solid-State NMR of Oriented Bicelles

Tuo Wang and Mei Hong*
Department of Chemistry, Massachusetts Institute of Technology, 170 Albany Street, Cambridge, MA 02139

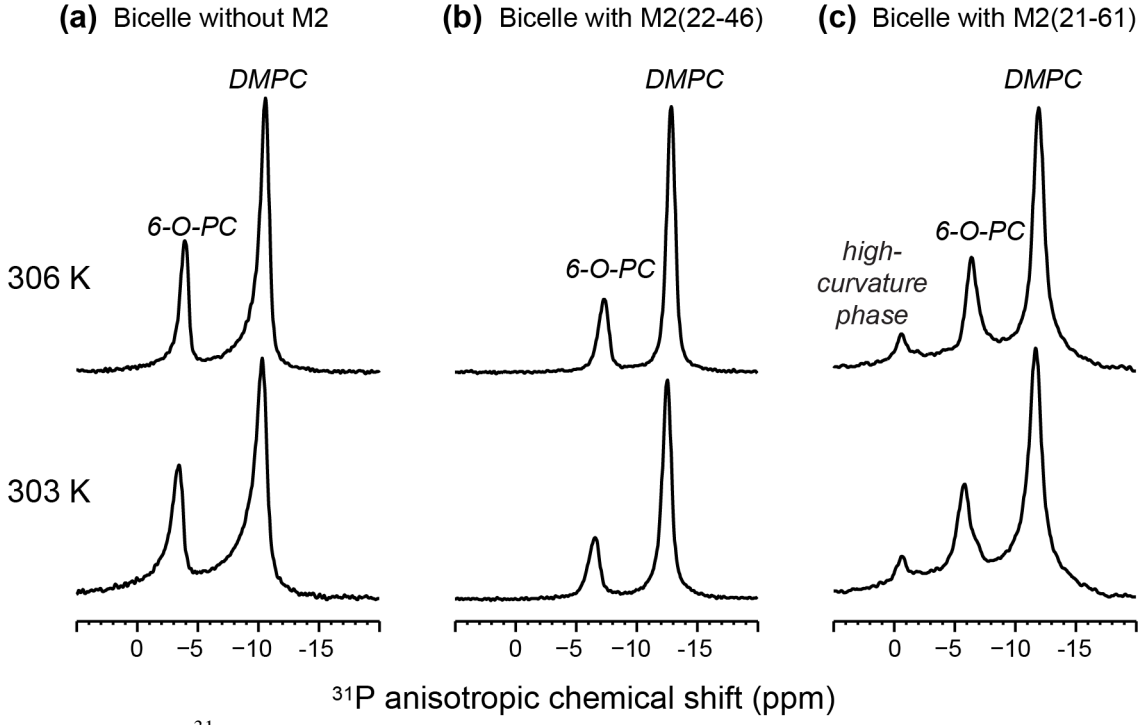

Figure S1. Static ^{31}P spectra of DMPC/6-O-PC bicelles. (a) Control sample without M2. (b) M2(22-46)-containing bicelles. (c) M2(21-61)-containing bicelles. M2(21-61) causes an isotropic peak that is absent in the M2(22-46) sample.

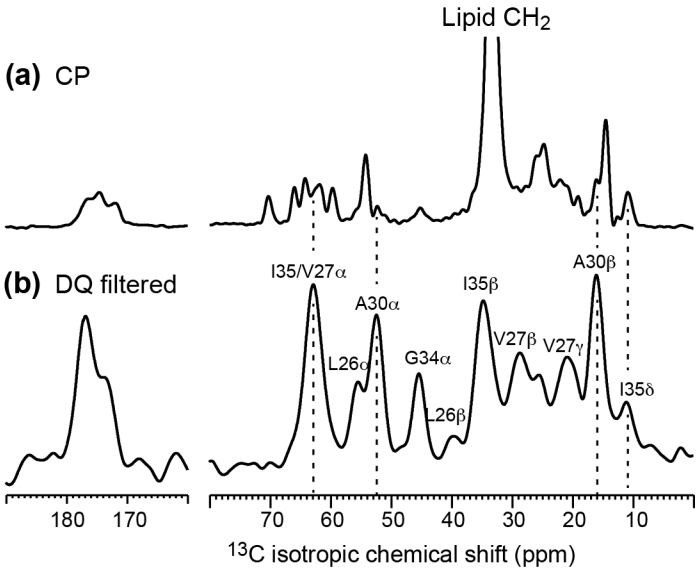

Figure S2. 1D ^{13}C CP (a) and double-quantum filtered (b) spectra of M2(21-61)-containing DMPC/DHPC bicelles at 253 K under 5 kHz MAS. The ^{13}C isotropic chemical shifts of the TM residues correspond to α-helical conformations, indicating that the TM domain adopts the same helical structure in the bicelle as in multilamellar liposomes.

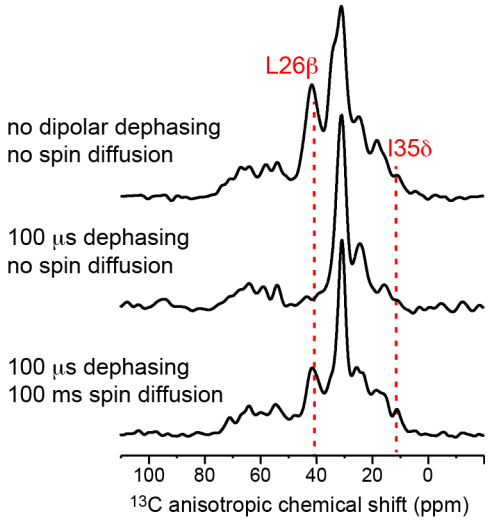

Figure S3. Dephasing of peptide signals by ^{13}C-^{1}H dipolar coupling. A 100 μs dipolar filter removed the L26 Cβ signal and significantly suppressed the I35 Cδ1 intensity. A mixing period (t_m) of 100 ms restored the peptide ^{13}C signals by transferring ^{1}H magnetization from lipids to peptide.